Rapidly dynamic host cell heterogeneity in bacterial adhesion governs susceptibility to infection by *Listeria monocytogenes*

Michelle Rengarajan[a] and Julie A. Theriot[b],*
[a]Department of Medicine, Massachusetts General Hospital, Boston, MA 02114; [b]Department of Biology, University of Washington, Seattle, WA 98185-1800

ABSTRACT Interactions between host cells and individual pathogenic bacteria determine the clinical severity of disease during systemic infection in humans. Vascular endothelial cells, which line the lumen of blood vessels, represent a critical barrier for a bacterium in the bloodstream. These cells adopt a myriad of phenotypes that may modulate their susceptibility to infection; however, the precise determinants of their heterogeneity in susceptibility are not known. Here, we show that heterogeneity in susceptibility to *Listeria monocytogenes* infection among primary human vascular endothelial cells can be attributed entirely to robust, preexisting host cell heterogeneity in bacterial adhesion, and we find no evidence for significant heterogeneity in later steps of infection. High susceptibility to adhesion decays rapidly, within 30–60 min. Thus, rapidly fluctuating, nongenetic variability in bacterial adhesion diversifies susceptibility to infection, both among host cells and within individual cells over time.

INTRODUCTION

Genetically identical cells grown under identical conditions exhibit substantial cell-to-cell variation in behavior based on fluctuations in gene expression (Spudich and Koshland, 1976). Recent advances in analysis of gene expression and protein levels in single cells have demonstrated that this phenomenon is widespread in mammalian cells as well as bacteria, and has broad biological significance (Loewer and Lahav, 2011; Snijder and Pelkmans, 2011). In microbial pathogenesis, nongenetic heterogeneity in both host cells (Snijder *et al.*, 2009) and infecting pathogens (Avraham *et al.*, 2015) can contribute to extreme variation in the outcome of infection (Garcia-Del Portillo, 2008).

Host cell invasion by intracellular pathogens requires a complex multistep process; variation among host cells or bacteria that affects any step may influence susceptibility to infection. Infection by the Gram-positive facultative intracellular pathogen *Listeria monocytogenes* represents a particularly interesting case because this bacterium has a complex and well characterized infectious cycle (Portnoy *et al.*, 2002) that relies heavily on active participation by the host cell for initial invasion (Mengaud *et al.*, 1996) as well as for subsequent intracellular actin-based motility (Tilney and Portnoy, 1989) and cell-to-cell spread (Robbins *et al.*, 1999). We have previously shown that primary human vascular endothelial cells (HUVEC) take up *L. monocytogenes* in a phagocytosis-like process that is independent of specific bacterial virulence factors (Rengarajan *et al.*, 2016). Here, we describe robust, rapidly dynamic heterogeneity in the susceptibility of HUVEC to *L. monocytogenes* infection that appears to be entirely governed by the very first step of infection: bacterial adhesion to the host cell surface.

RESULTS AND DISCUSSION

To quantify heterogeneity in susceptibility to bacterial infection, we exposed HUVEC to a 1:1 mixture of otherwise isogenic *L. monocytogenes* that constitutively expressed one of two fluorescent proteins, either mTagRFP (strain JAT1070), referred to here as red bacteria, or mVenus^{R80Q} (strain JAT1072), referred to here as green bacteria. Over a range of multiplicities of infection (MOI, ratio of bacteria in inoculum to total number of host cells) from ~1 to ~2000, the invasion efficiency of these two strains was roughly comparable (Figure 1A; see *Materials and Methods*). If infection events are independent, and all cells are equally susceptible to infection, then

FIGURE 1: HUVEC exhibit heterogeneity in susceptibility to infection by *L. monocytogenes*. (A) Dependence of HUVEC infection on MOI. HUVEC were infected with a 1:1 mixture of mRFP- and mVenus^{R80Q}-expressing bacteria (red and green, respectively), with MOI for each strain from ~4 to ~2000. Observed percentage of HUVEC infected with each strain is shown as a function of MOI of that particular strain. The relationship between MOI and the fraction of HUVEC infected is similar for both strains. Inset shows the same data visualized in a semilog plot. (B) Hypothetical outcomes when HUVEC are infected with a 1:1 mixture of otherwise genetically identical bacteria expressing different fluorescent proteins. Top: Infection events are positively correlated: $f_{both} > f_{red}f_{green}$. Middle: Bacterial infection events are independent: $f_{both} = f_{red}f_{green}$. Bottom: Infection events are negatively correlated: $f_{both} < f_{red}f_{green}$. (C) Schematic for experiment in which HUVEC are infected with a mixture of otherwise identical red or green bacteria. The antibiotic gentamicin (gent.) is added to kill extracellular (but not intracellular) bacteria, thereby stopping further bacterial internalization (Havell, 1986; Portnoy *et al.*, 1988). (D) Enrichment for multiply infected HUVEC. HUVEC were infected with a 1:1 mixture of red and green bacteria as detailed in C. Data from one sample are plotted as a histogram of HUVEC RFP fluorescence. Bar graph shows percent of HUVEC infected with red bacteria among total cells (gray bar) and among cells infected with green bacteria (green bar), with enrichment in the latter population. (E) Bacterial infection events are positively correlated. HUVEC were infected with a 1:1 mixture of red and green bacteria as in C, D. Observed percentage of HUVEC infected with both strains of bacteria (f_{both}, *y*-axis) is plotted against expected percentage of HUVEC infected with both strains of bacteria assuming independence ($f_{red}f_{green}$), with each point colored to indicate the total (red and green) bacterial MOI to which HUVEC were exposed. Each data point represents an independent sample, with data collected from five independent experiments performed on different days. Varying MOI across nearly four orders of magnitude allowed variation in both the expected and observed percentages of HUVEC infected with both bacteria, which demonstrates how enrichment for multiply infected cells varies as a function of the expected percentage infected with both bacteria. Inset is the same data, magnifying lower values in the curve, where the distance from the expected values is greatest.

the proportion of HUVEC infected with both strains of bacteria (f_{both}) should be the product of the proportion infected with red bacteria (f_{red}) and the proportion infected with green bacteria (f_{green}): $f_{both} = f_{red} \times f_{green}$ (Figure 1B). In contrast, if infection with one bacterium inhibits subsequent infection of the same cell with another bacterium, $f_{both} < f_{red} \times f_{green}$. This phenomenon, frequently observed in viral infections, is referred to as superinfection exclusion (Bennett, 1953; Folimonova, 2012). If infection with one bacterium promotes infection with additional bacteria, or if some HUVEC are more susceptible to infection than others, $f_{both} > f_{red} \times f_{green}$ (Figure 1B). Experimentally, we measured f_{both}, f_{red}, and f_{green} on a cell-by-cell basis using flow cytometry 6 h after bacterial exposure (Figure 1C), as previously described (Rengarajan et al., 2016). After exposure to both red bacteria and green bacteria, f_{red} was higher within the population of host cells also harboring green bacteria than in the total host cell population (Figure 1D); that is, the host cell population was enriched for HUVEC infected with both bacterial strains. Indeed, across a wide range of MOI, we consistently saw $f_{both} > f_{red} \times f_{green}$ (Figure 1E).

These data suggest either that bacterial infection enhances the propensity of HUVEC for additional superinfection by other bacteria (Model 1) or that HUVEC are heterogeneous in their preexisting susceptibility to infection (Model 2) (Figure 2A). To distinguish between these models, we exposed HUVEC to red bacteria immediately before exposing them to green bacteria. In Model 1 (Figure 2A, top), all HUVEC are initially equally susceptible to infection. Red bacteria infect a random subset of HUVEC and increase the susceptibility only of the red-infected cells. The remaining cells that were exposed to, but not infected by, red bacteria would have the same susceptibility to subsequent invasion as a naïve population that was not exposed to red bacteria. In contrast, in Model 2 (Figure 2A, bottom), HUVEC are initially heterogeneous in susceptibility to invasion. Red bacteria infect the most susceptible cells at a high rate; these most susceptible cells are removed from the uninfected population, so that the remaining population of cells that were exposed to but not infected by red bacteria will be *less* susceptible to subsequent bacterial invasion than a naïve population. Indeed, we found that the proportion of HUVEC infected with green bacteria was higher for a naïve population than for the population exposed to, but not infected with, red bacteria (Figure 2B), demonstrating that heterogeneity in susceptibility of HUVEC to infection results from preexisting HUVEC heterogeneity in susceptibility, compatible with Model 2.

L. monocytogenes infection is a multistep process, with initial bacterial adhesion to host cells followed by internalization of adhered bacteria, escape from the membrane-bound vacuole, and replication in the cytoplasm. To clarify when enrichment for multiply infected cells within the multistep infection process, we examined the kinetics of *L. monocytogenes* uptake by exposing HUVEC to bacteria at MOI of ~2–150 bacteria per host cell for 10–150 min. The rate of infection was MOI-dependent only in the first 10 min after bacterial exposure (Supplemental Figure S1, A–C). Additionally, when we exposed HUVEC to varying doses of a 1:1 mixture of red and green bacteria for 10–150 min, increasing exposure time did not significantly change the shape of the enrichment curve (Supplemental Figure S1, D and E). Thus, positive correlation between infection events is established within the first 10 min of bacterial exposure, corresponding to the time frame of initial bacterial adhesion to the host cell and subsequent internalization.

To examine directly whether adhesion or internalization exhibited positive correlation with heterogeneity, we used inside/outside staining (Yam and Theriot, 2004; Rengarajan et al., 2016) to count the exact number of adhered and internalized *L. monocytogenes* per HUVEC 30 min after exposure, before significant intracellular replication could occur. If susceptibility to bacterial adhesion were homogeneous, then the distribution of adhered bacteria per HUVEC should follow a Poisson distribution with the variance of the distribution equal to the mean, whereas a heterogeneous or clustered distribution should show an excess number of cells with high numbers of bacteria or with none at all (Clarke, 1946). Indeed, the variance of the distribution of adhered *L. monocytogenes* per HUVEC was consistently much greater than the mean (Supplemental Table S1), and the overall distribution of adhered bacteria per HUVEC was poorly fitted by a single-parameter Poisson distribution (Figure 3A), specifically because an excess number of host cells had large numbers of adhered bacteria. However, we noticed that the distribution of adhered bacteria per cell was well fitted by a negative binomial distribution (Figure 3A), a two-parameter model in which data are modeled as a sum of a series of Poisson distributions, each of whose representations is determined by a gamma distribution. These observations are consistent with a model in which HUVEC susceptibility for adhesion of *L. monocytogenes* effectively varies from cell to cell along a continuum. Consistent with such a model, the proportion of HUVEC that are infected did not exhibit a sharp phase transition at a particular MOI, but instead followed a smooth curve (Figure 1A). Similarly, the distribution of internalized bacteria per cell was also well fitted by a negative binomial distribution (Figure 3B; Supplemental Table S1).

Given that adhesion precedes internalization, it is possible that adhesion is heterogeneous from cell to cell but that all adhered bacteria have an equal probability of subsequent internalization across all host cells. Indeed, with this sole assumption, the distribution of adhered bacteria per cell closely predicted the actual distribution of internalized bacteria per cell (Figure 3C). Furthermore, our microscopy data for heterogeneous enrichment of bacterial adhesion and internalization at 30 min after bacterial exposure follow a pattern that is perfectly consistent with the standard enrichment curve that we previously determined using flow cytometry 5.5 h later in the infection process (Figure 3D).

Thus, the pattern of enrichment for multiply infected cells can be predicted by the distribution of internalized bacteria per cell, which in turn can be predicted by the distribution of adhered bacteria per cell. Importantly, these results strongly suggest that heterogeneity in *L. monocytogenes* infection of HUVEC results entirely from heterogeneity in the susceptibility of HUVEC to *L. monocytogenes* adhesion, and that all subsequent steps (internalization, escape from the vacuole, and replication within the cytoplasm) are independent and occur homogeneously throughout the HUVEC population.

If HUVEC heterogeneity in susceptibility to bacterial adhesion explains susceptibility to infection, then we should be able to quantitatively explain our flow cytometry data (Figure 1, A and E) with a mechanistic model that assumes only preexisting heterogeneity in susceptibility to infection among HUVEC. One striking feature of the observed quantitative relationship between MOI and percentage of HUVEC infected is its shallow slope; increasing the MOI from 100 to 200 (well below saturation) typically increased the number of infected HUVEC only 1.22-fold rather than the twofold that might be expected (SD = 0.08, n = 10). We used a stochastic simulation to estimate the fraction of host cells that would be infected over a range of MOI from 1 to ~2200 for each strain (matching the range of data available), and found that it was not possible to fit the experimental data using any model where all host cells were assumed to be equally susceptible to infection (Figure 3E, purple curves). However, the data were well fitted by the same
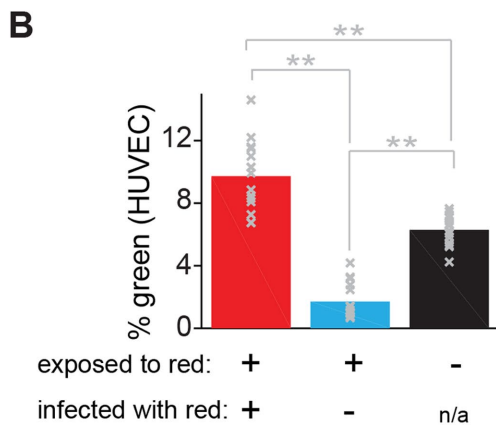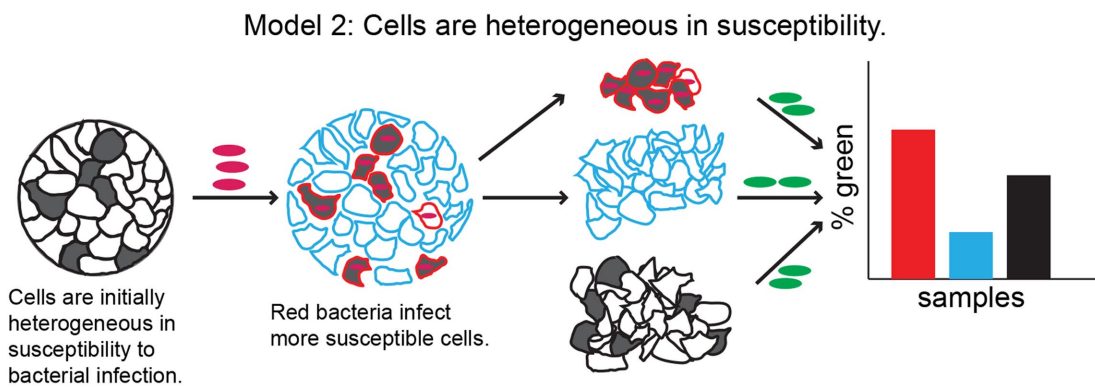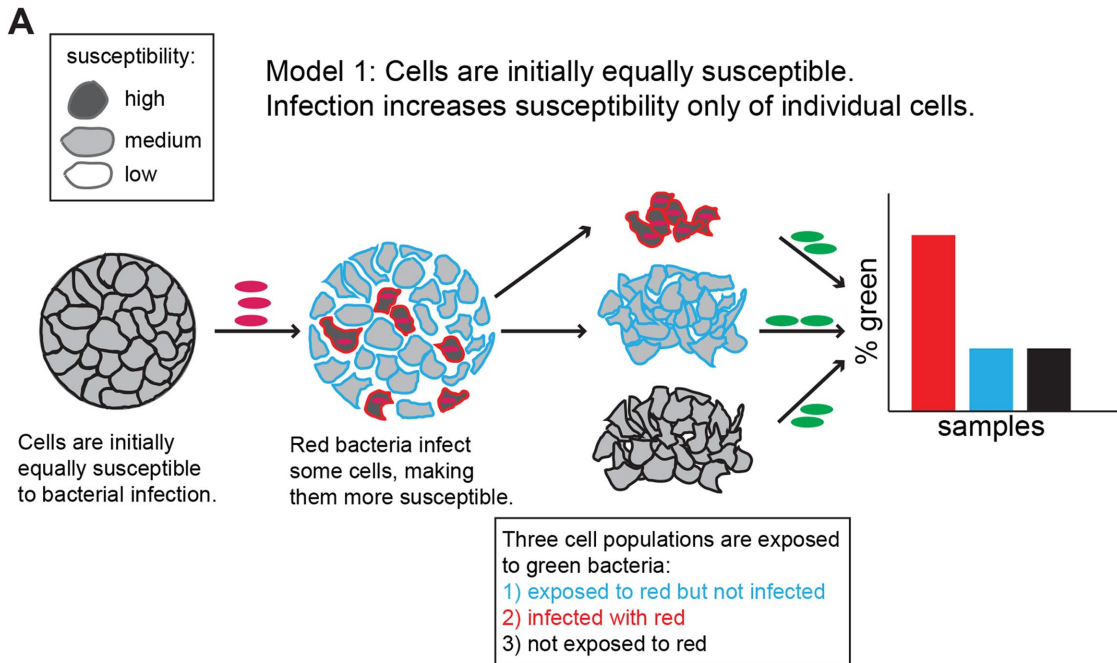
FIGURE 2: Preexisting endothelial cell heterogeneity establishes heterogeneity in infection with *L. monocytogenes*. (A) Possible models to generate enrichment for multiply infected cells. (B) Naïve HUVEC (black) are more likely to be infected with green bacteria than cells that were previously exposed to but not infected with red bacteria (blue). One population of HUVEC was exposed to red bacteria (MOI ~1600) for 10 min, and then unbound red bacteria were washed off and HUVEC were exposed to green bacteria (MOI ~1500) for 10 min. A second population (black bar) was only exposed to green bacteria. Data are shown as mean (bars) with individual data points overlaid (gray *x*'s). *p*-values for pairwise comparisons (unpaired two-sided, two-sample *t*-test, Benjamini–Hochberg correction for multiple hypothesis testing): <0.00001 (naïve vs. exposed to RFP but uninfected), 0.00007 (naïve vs. infected with RFP), <0.00001 (exposed to, but not infected with, RFP vs. infected with RFP).

simulation with the assumption that the host cells were variable in their susceptibility, where the underlying susceptibility followed a gamma distribution, reproducing the shallow slope of the experimental data curve as well as the steeper slope at very low MOI (Figure 3E, black curve). We determined the two parameters of the gamma distribution that best fit this experimental data on the fraction of host cells infected as a function of MOI (see *Materials and Methods*).

We then used this same stochastic model to simulate a mixed infection using equal numbers of red and green bacteria and calculated the enrichment curve as defined above. Importantly, because we have already set the gamma distribution parameters using data on the fraction of host cells infected as a function of MOI (Figure 3E), there are no remaining free parameters in the model. Impressively, the simulation matched the observed data well over the entire range (Figure 3F). Thus, our anomalous quantitative observations on the relationship between MOI and fraction of host cells infected and on the excess enrichment of host cells infected by two different bacterial strains, as well as the non-Poisson distribution of adherent and internalized bacteria shortly after exposure, are all consistent with the same very simple underlying model, in which HUVEC have a preexisting broad distribution of susceptibilities to bacterial adhesion. In addition, we examined the effects on enrichment of other plausible distributions of intrinsic host cell susceptibility (Supplemental Figure S2). Although the parameter-free gamma model provided the closest match to the experimental data, any distribution where some subset of cells is substantially more susceptible than the population average can give some positive enrichment.

It is possible that population-wide gene expression changes that modulate the average susceptibility of HUVEC could also change the enrichment pattern for multiply infected cells. Our mechanistic model predicted that changing only the average susceptibility of the HUVEC population should only change the position of data along the enrichment curve and not the shape of the curve (Figure 4A). We have previously found that siRNA depletion of the Rho GTPase guanine nucleotide exchange factor (GEF) GEF-H1 decreases bacterial invasion (Rengarajan *et al.*, 2016); however, depletion of GEF-H1 did not affect enrichment for multiply infected cells (Figure 4, B and C). Similarly, depletion of a distinct Rho GEF, LARG, which increased overall infection, also had no effect on enrichment (Figure 4, B and C).

High susceptibility to bacterial adhesion could represent either a stable or a transient cellular state. To differentiate between these two possibilities, we exposed host cells to red bacteria and subsequently to green bacteria after a variable time delay. We found that high susceptibility was transient and decayed on a time scale of roughly 1 h (Figure 4D). Notably, cell-to-cell variability in the levels of many proteins has previously been shown to decay on a time scale of ~40 h (Sigal *et al.*, 2006). Given this substantial difference in time scale, variation in gene expression between cells is unlikely to explain heterogeneity in susceptibility to bacterial adhesion. This particular form of heterogeneity might result from rapidly fluctuating changes in the activity (rather than the expression level) of host proteins involved in invasion of *L. monocytogenes*, as cell signaling can vary over much shorter timescales than protein expression (Jeschke *et al.*, 2013, Purvis and Lahav, 2013). Alternatively, nonprotein cell surface components, such as the glycocalyx, might be significantly variable contributors to bacterial adhesion.

The rapid kinetics associated with susceptibility to infection suggests that an individual host cell can change its degree of susceptibility over a time scale comparable to a single human exposure event, typically the consumption of a single meal including food contaminated with *L. monocytogenes* (Farber and Peterkin, 1991). Rapidly fluctuating susceptibility may enhance infection in vivo by increasing the probability that some cells are hypersusceptible to infection at any given time. Because *L. monocytogenes* can harness a host cell's actin to spread rapidly from cell to cell, direct invasion of even a single cell in a cellular sheet can promote more substantial infection within that sheet of cells (Tilney and Portnoy, 1989; Robbins *et al.*, 1999). Thus, by increasing the prevalence of even a small number of hypersusceptible cells, heterogeneity in susceptibility of individual cells may increase the susceptibility of a cellular sheet in vivo within changing the average susceptibility of the cells within that sheet.

By examining the infection cycle of *L. monocytogenes* in host cells using quantitative assays at multiple points, we have demonstrated that essentially all of the apparent heterogeneity in bacterial infection of HUVEC arises from heterogeneity in initial adhesion, with subsequent steps (internalization, escape from the vacuole, and replication in the cytoplasm) likely acting independently without significant cell-to-cell variation. Intriguingly, we have previously shown that while adhesion of bacteria or beads to HUVEC is differentially regulated, subsequent internalization may follow a common cargo-independent mechanism (Rengarajan *et al.*, 2016); thus, specifically modulating adhesion may confer flexibility in uptake of multiple types of cargo by endothelial cells. Although we have been able to estimate the time scale of adhesion variation in this system as about 1 h, we do not know the molecular mechanism responsible for this variation. Because our assay for adhesion variation necessarily required exposure to infectious bacteria, we cannot determine whether bacterial exposure itself might contribute to the observed heterogeneity or its temporal variation. The simple but revealing experimental approach that we have developed using differentially tagged but otherwise identical bacterial strains should be generally adaptable to explore similar questions on the origins of heterogeneity in infection for other bacterial and viral pathogens, as well as *L. monocytogenes*.

MATERIALS AND METHODS

Bacterial strain construction and cell culture
Bacterial strains and plasmids used in this study are listed in Supplemental Table S2. For constitutive fluorophore expression, mVenus^{R80Q} or codon-optimized mTagRFP (Zeldovich *et al.*, 2011) were cloned into the vector pMP74 (in place of GFPmut2; Pentecost *et al.*, 2010) to generate vectors pMR01 and pMR02, in which mVenus^{R80Q} (a gift from the Shapiro lab) and mTagRFP, respectively, were expressed under the control of the Hyper-SPO1 promoter fused to the 5′ UTR of hly (Shen and Higgins, 2005; Pentecost *et al.*, 2010). All constructs were made by Epoch Life Science. To express fluorescent proteins in *L. monocytogenes* strains, plasmids were transformed into *E. coli* SM10 λ pir and subsequently transferred to *L. monocytogenes* by conjugation (Lauer *et al.*, 2002). Constructs were stably integrated into the tRNA^{ARG} locus of the bacterial chromosome as previously described (Lauer *et al.*, 2002). *L. monocytogenes* and HUVEC were cultured as previously described (Rengarajan *et al.*, 2016).

Antibodies
The primary antibody used for inside/outside staining was rabbit anti-*Listeria monocytogenes* (Meridian Life Science B65420R).

Endothelial cell infection and analysis
We previously showed that exposure to extracellular listeriolysin O, the *L. monocytogenes* pore-forming toxin, causes HUVEC death
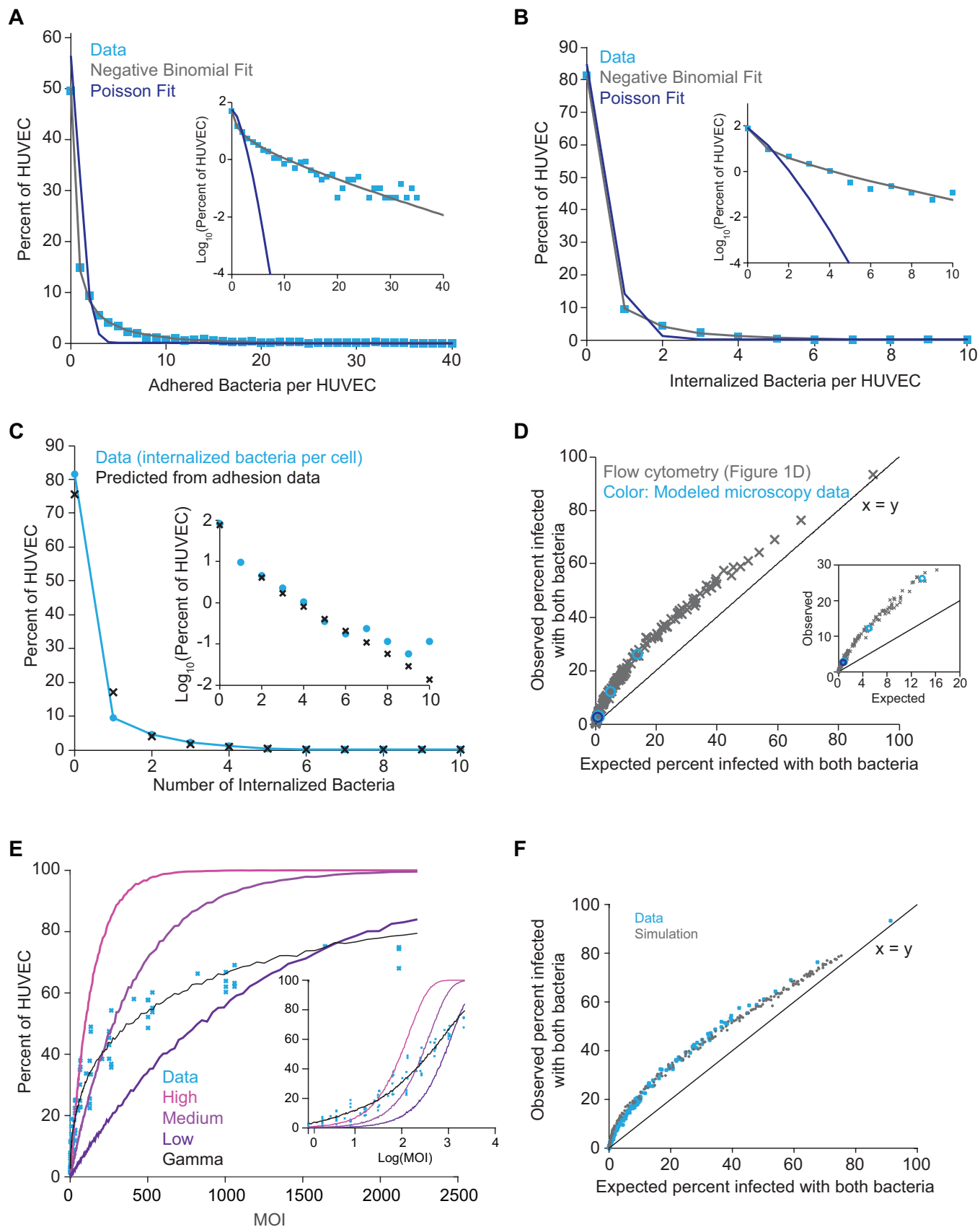
FIGURE 3: Heterogeneity in infection of endothelial cells with *L. monocytogenes* is established by heterogeneous bacterial adhesion. (A) Distribution of adhered bacteria per HUVEC (n = 1728 HUVEC, MOI: 40), determined by inside/outside staining. The distribution is well fitted by a negative binomial distribution $P\{x|r,p\} = \dfrac{\Gamma(r+x)}{(r)\Gamma(x+1)} p^r (1-p)^x$, where

during initial exposure to high bacterial titers in culture; a listeriolysin O point mutation, LLO^(G486D), with decreased hemolytic activity does not cause such early cell death and can support the full *L. monocytogenes* infectious cycle during infection with HUVEC (Rengarajan *et al.*, 2016). Therefore, all endothelial cell infections in this study were performed in an LLO^(G486D) background strain. Endothelial cells were exposed to *L. monocytogenes* as previously described (Rengarajan *et al.*, 2016); nonadherent bacteria were removed by washing 30 min after bacterial exposure and 20 µg/ml gentamicin was added 1 h after exposure to stop new bacterial uptake. For kinetics experiments, washes were performed and gentamicin was added 10–150 min after bacterial exposure, as indicated in Supplemental Figure S1. For all experiments, MOI was quantified directly by plating serial dilutions of the bacterial inoculum.

To evaluate the relative infection efficiency and relative enrichment of green (mVenus^(R80Q)) and red (mTagRFP) strains, mixed infections were performed on five separate days with a range of MOI from ~1–3 on the low end to ~1500–2200 on the high end. Infection was analyzed by flow cytometry 6 h after exposure (2500–5000 cells per sample; Rengarajan *et al.*, 2016), quantifying numbers of host cells infected by green only, red only, or both green and red bacteria. To analyze infection efficiency, plots of log(MOI) versus fraction of host cells infected with each strain were constructed independently for each experimental day, and linear fits were calculated for the appropriate near-linear range of this curve (typically MOI 10–1000); then fraction infected was interpolated for MOI = 100. Overall, red bacteria had a slight infection advantage over green bacteria, resulting in an average of 0.11 higher fractional infection efficiency at MOI = 100 (SD = 0.07, $n = 5$).

For experiments on early stages of infection, analysis was performed by inside/outside staining 30 min after exposure (500–1000 cells per sample; Yam and Theriot, 2004). To quantify internalized or adherent bacteria by inside/outside staining, all bacteria associated with individual HUVEC were counted as adherent; bacteria that lacked the "outside" stain (applied before permeabilization) were counted as internalized.

To determine the effect of siRNA depletion of GEF-H1 or LARG (Figure 4C) on average susceptibility, 300–500 images per condition were captured on an ImageXpress Micro (Molecular Devices) using a 10× air objective and analyzed as previously described (Rengarajan *et al.*, 2016).

siRNA perturbations were performed as previously described (Rengarajan *et al.*, 2016) using synthetic siRNA pools from Dharmacon (LARG SMARTpool: ON-TARGETplus Human ARHGEF12 siRNA L-008480-00, GEF-H1 SMARTpool: ON-TARGETplus Human ARHGEF2 siRNA L-009883-00, control: ON-TARGETplus Non-targeting Pool D001810-10).

Prediction of the distribution of internalized bacteria per cell from the distribution of adhered bacteria per cell

If heterogeneity in bacterial adhesion to HUVEC is the primary source of heterogeneity in infection, then the distribution of internalized bacteria per cell may deviate from a Poisson distribution (Figure 3B) only because the distribution of adhered bacteria per cell deviates from a Poisson distribution (Figure 3A), and internalized bacteria are a subset of adhered bacteria. In this case, the probability of internalization should be the same for all adhered bacteria, regardless of the individual HUVEC to which a bacterium is adhered. Thus, for our data,

$$P(\text{internalization of adhered bacteria}) = p_{IIA}$$

$$= \frac{\text{total number of internalized bacteria}}{\text{total number of adhered bacteria}} = \frac{677}{3046} = 0.2223$$

It follows that for $n > 0$,

$$p_n = \sum_{m=n}^{\infty} P_m \frac{m!}{n!(m-n)!} p_{IIA}^n (1 - p_{IIA})^{m-n}$$

where p_n is the probability that a given HUVEC has exactly n internalized bacteria and P_m is the probability of having m bacteria adhered. A cell with 0 adhered bacteria must have 0 internalized bacteria; therefore,

$$p_{n=0} = P_{m=0} + \sum_{m=1}^{\infty} P_m (1 - p_{IIA})$$

Notably, as derived above, the predicted distribution of internalized bacteria per cell closely predicted the actual measured distribution of internalized bacteria per cell using only parameters that are directly measured from the data; no fitting is necessary (Figure 3C). Thus, we conclude that heterogeneity among HUVEC in internalization of bacteria derives primarily from heterogeneity among HUVEC in adhesion of bacteria.

$r = 0.32$, $p = 0.11$). (B) Distribution of internalized bacteria per HUVEC from the same experiment as shown in A determined by inside/outside staining. The distribution is well fitted by a negative binomial of the same form, with parameters $r = 0.17$, $p = 0.31$. (C) The distribution of internalized bacteria per cell can be predicted from the distribution of adhered bacteria per cell. The measured distribution of internalized bacteria per cell (blue) is well approximated by a model in which we assume that all adhered bacteria were equally likely to invade (black; see *Materials and Methods* for details of the calculation). (D) The enrichment curve for multiply infected bacteria generated from flow cytometry experiments for which infection is analyzed after 6 h (gray) corresponds well to the distribution of bacteria per cell generated in microscopy experiments for which infection is analyzed after 30 min (blue dots, with one point shown in dark blue, as it nearly superimposes another data point). To calculate where microscopy data falls on these axes, for the *y*-axis we calculate the "observed" percentage infected with both bacteria from the experimentally determined distribution of bacteria per cell (see *Materials and Methods* for details of the calculation) and assume that each counted bacterium is equally likely to be red or green. The "expected" percentage on the *x*-axis was estimated by assuming a Poisson distribution of bacteria per cell, fit to the uninfected fraction of the actual data. (E) Stochastic simulations were performed as described in *Materials and Methods* to explore the effect of defined susceptibility in HUVEC infection. Host susceptibility was simulated as constant across the host cell population (purple curves, for high-, medium-, and low-susceptibility populations) or as variable across the host cell population with gamma-distributed susceptibility (black curve). Data (from Figure 1A) are plotted as MOI versus percent of HUVEC infected, with lines representing simulations. Gamma-distributed heterogeneous susceptibility best fits the data. (F) Stochastic simulations were performed as in E with gamma-distributed susceptibility to infection and simulation of infection with both red and green bacteria. Data are plotted as $f_{red}f_{green}$ (*x*-axis) versus f_{both} for standard data from Figure 1E (blue) or simulation (gray).
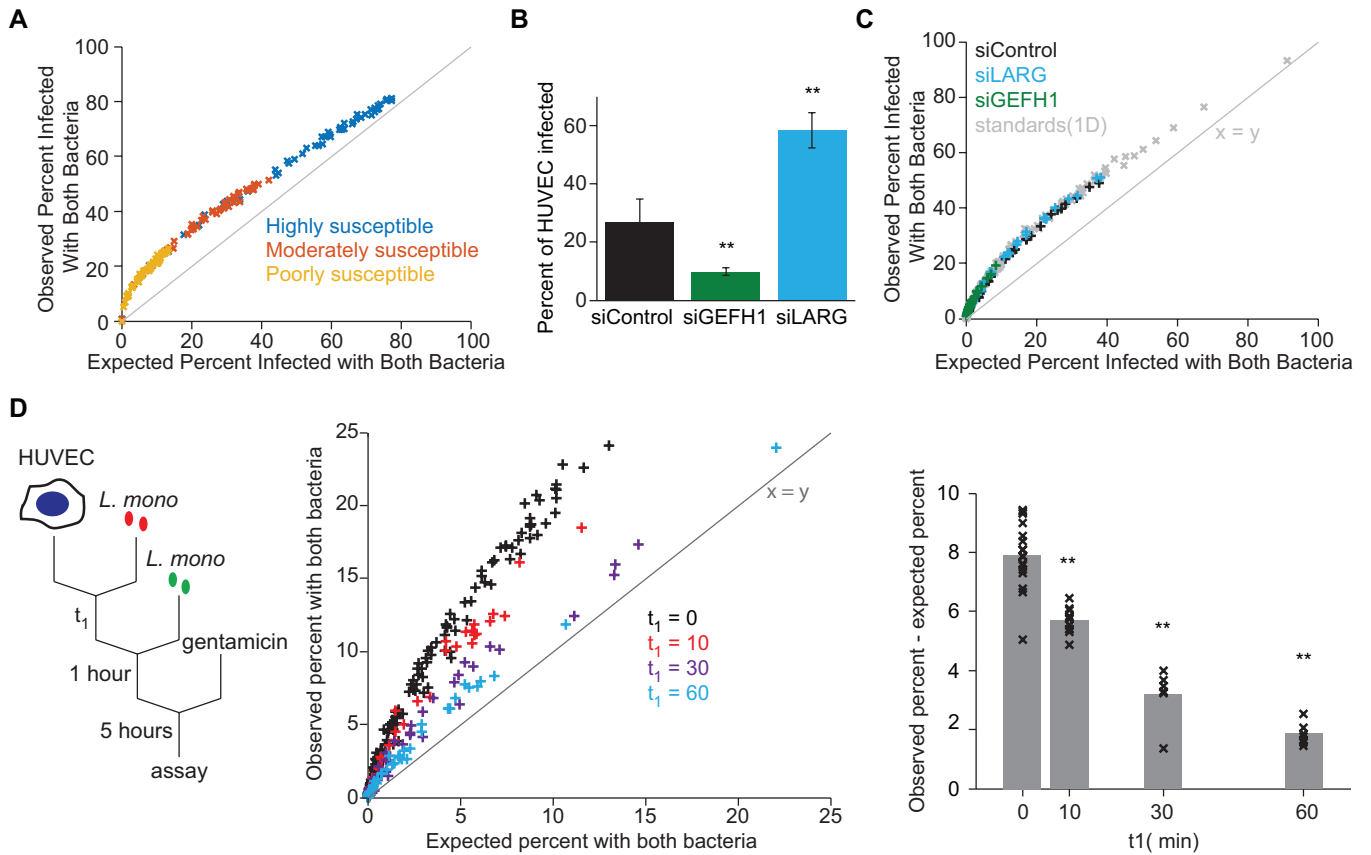
FIGURE 4: High susceptibly of HUVEC to infection with *L. monocytogenes* decays rapidly. (A) Stochastic simulations were performed as in Figure 3F. Host susceptibility across the host cell population was simulated as variable along a gamma distribution. To generate populations of host cells with different average susceptibility, the scale parameter of the gamma distribution was varied 25-fold (1000, 5000, 25,000 for low, medium, and high susceptibility, respectively). Simulations predict that changing the average susceptibility of the HUVEC population to infection changes the position of data along the curve but not the shape of the curve. (B) Depleting modulators of Rho GTPase can alter average population HUVEC infection in opposing directions. HUVEC were treated with siRNAs targeting either the RhoGEF LARG (*ARHGEF12*) or the RhoGEF GEF-H1 (*ARHGEF2*) or nontargeting control siRNA (NT). HUVEC were exposed to *L. monocytogenes* (JAT983; MOI: 43). Infection was assayed by microscopy (mean ± SD, $n = 4$ biological replicates), 8 h after infection. *p*-values for each sample relative to siNT control (unpaired two-sided, two-sample *t*-test, Benjamini–Hochberg correction for multiple hypothesis testing): 0.025 (GEF-H1), 0.007 (LARG). Data for GEF-H1 and control have previously been published in Rengarajan *et al.* (2016). (C) Depleting GEF-H1 or LARG has no effect on enrichment for highly susceptible cells. HUVEC were treated with siRNAs targeting LARG or GEF-H1 or nontargeting control siRNA, then exposed to red or green *L. monocytogenes* (MOI each: 8-550) as in Figure 1, C–E. Each point represents an independent sample. Observed and expected percentages of cells infected with both strains of bacteria are determined as in Figure 1E. Enrichment for observed value of f_{both} relative to expected value is not significant (*p*-values for each sample relative to siNT control were calculated as detailed below in D, with unpaired two-sided, two-sample *t*-test, Benjamini–Hochberg correction for multiple hypothesis testing: 0.84 [siLARG], 0.13 [siGEF-H1]). (D) Left: Representation of sequential bacterial addition experiments. The time between separate addition of red and green bacteria (t_1) ranges from 0 to 60 min. Middle: Observed percent of cells infected with both colors as a function of the expected fraction, calculated as in Figure 1E, when green bacteria were added 0 (black), 10 (red), 30 (purple), or 60 (blue) minutes after red bacteria. Right: To compare samples, data from middle panel were filtered to include only points for which $0.04 < f_{red}f_{green} < 0.07$ to control for variations in the shape of the enrichment curve across values of $f_{red}f_{green}$. For each data point in this smaller data set, $f_{both} - f_{red}f_{green}$ was calculated. Data are plotted as mean($f_{both} - f_{red}f_{green}$) for each value of t_1 (gray bars) with individual data points (black *x*'s) overlying. Corrected *p*-values for pairwise comparisons to $t_1 = 0$ (unpaired two-sided, two-sample *t*-test, Benjamini–Hochberg correction for multiple hypothesis testing): <0.00001 ($t_1 = 10$), <0.00001 ($t_1 = 30$), <0.00001 ($t_1 = 60$).

Calculation of correlation between enrichment (flow cytometry) and distribution of bacteria per cell (microscopy)

For each data point (four points shown in blue in Figure 3D), we started with the measured distribution of bacteria per cell, determined by inside/outside staining. For a given cell with n total bacteria, we assumed that the number of green bacteria in the cell was

determined by the binomial distribution. Then, for each individual HUVEC, the probability that there are exactly k green bacteria in that cell ($P_g(X = k)$) was given by

$$P_g(X = k) = \frac{n!}{k!(n-k)!}p^k(1-p)^{n-k} \qquad (1)$$

where n is the number of internalized bacteria and p is the probability that an internalized bacterium is green. In the data shown in Figure 1E, we infected cells with a 1:1 mixture of red and green bacteria. Given comparable infection efficiency for the two strains as described above, we assumed that $p = p_{green} = p_{red} = 0.5$.

The probability that an individual HUVEC has both red and green bacteria (P_{both}) is simply the probability that $1 \le k \le n\text{-}1$, that is, the probability that there is at least 1 green bacterium and at least 1 bacterium that is not green:

$$p_{both} = P_g \ (1 \le X \le n-1) = 0.5^n \sum_{k=1}^{n-1} \frac{n!}{k!(n-k)!} \tag{2}$$

If the number of HUVEC infected with n bacteria is given by $\propto_n$, and the number of bacteria in an individual HUVEC can itself vary from 0 to ∞, then the total number of HUVEC in the population that are infected with both red and green bacteria (N_{both}) is given by

$$N_{both} = \sum_{n=0}^{\infty} \propto_n \times 0.5^n \times \sum_{k=1}^{n-1} \frac{n!}{k!(n-k)!} \tag{3}$$

and the total number of HUVEC in the population is $\sum_{n=0}^{\infty} \propto_n$.

Thus, the fraction of HUVEC predicted to be infected with both strains of *L. monocytogenes* (f_{both}) was determined from the known distribution of bacteria per HUVEC as follows:

$$f_{both} = \frac{\sum_{n=0}^{\infty} \propto_n \times 0.5^n \times \sum_{k=1}^{n-1} \frac{n!}{k!(n-k)!}}{\sum_{n=0}^{\infty} \propto_n} \tag{4}$$

For the predicted value of the percentage of HUVEC infected with both strains of bacteria (plotted on the y-axis in Figure 3D), we calculated f_{both} using the known $\propto_n$ from the measured distribution of the number of bacteria per cell. To calculate the "expected" percentage of HUVEC infected with both bacteria (x-axis in Figure 3D), we calculated f_{both}, assuming that $\propto_n$ follows a Poisson distribution (i.e., a condition in which uptake events were independent and all cells were equally susceptible to infection). We derived expected Poisson-distributed values for the number of bacteria per HUVEC as follows. To calculate λ, the single parameter of the Poisson distribution, we used the measured fraction of cells with 0 bacteria:

$$P(X = k) = \frac{(\lambda^k e^{-\lambda})}{k!} \tag{5}$$

$$\lambda = -\ln(f_{no\ bacteria}) \tag{6}$$

Stochastic simulation of bacterial infection

Simulations were performed using custom MatLab code. For each simulation, a number of host cells was selected (usually between 500 and 2000) for a range of MOI (typically between 1 and 3000), and each host cell was challenged with infection by a number of bacteria determined by a random Poisson draw from the current MOI. The likelihood of successful invasion for each bacterium was randomly determined based on the host cell's susceptibility. For simulations, susceptibility was defined as the number of bacteria necessary for a 50% likelihood of success, so low values of this parameter corresponded to extremely susceptible cells. For simulations shown in Figure 3E, the susceptibility values corresponding to high, medium, and low infection conditions were 70, 200, and 600. For the gamma-distributed susceptibility simulation in Figure 3, E and F, the shape parameter was chosen as 0.45 and the scale parameter as 2000. For simulations to change the average cell susceptibility with the gamma-distributed

susceptibility (Figure 4B), the scale parameter was varied fivefold (1000, 5000, 25,000 for low, medium, and high susceptibility, respectively) with shape parameter 0.45. For simulations using other distributions of host cell susceptibility (Supplemental Figure S2), all distributions were selected so that the average susceptibility was the same for all comparisons: constant (value = 900), two pools (values = 100 and 1700), uniform (from 1 to 1800), and exponential (lambda = 900).

REFERENCES
Avraham R, Haseley N, Brown D, Penaranda C, Jijon HB, Trombetta JJ, Satija R, Shalek AK, Xavier RJ, Regev A, Hung DT (2015). Pathogen cell-to-cell variability drives heterogeneity in host immune responses. Cell 162, 1309–1321.

Bennett CW (1953). Interactions between viruses and virus strains. Adv Virus Res 1, 39–67.

Clarke RD (1946). An application of the Poisson distribution. Journal of the Institute of Actuaries 72, 481.

Farber JM, Peterkin PI (1991). *Listeria monocytogenes*, a food-borne pathogen. Microbiol Rev 55, 476–511.

Folimonova SY (2012). Superinfection exclusion is an active virus-controlled function that requires a specific viral protein. J Virol 86, 5554–5561.

Garcia-Del Portillo F (2008). Heterogeneity in tissue culture infection models: a source of novel host–pathogen interactions? Microbes Infect 10, 1063–1066.

Havell EA (1986). Synthesis and secretion of interferon by murine fibroblasts in response to intracellular *Listeria monocytogenes*. Infect Immun 54, 787–792.

Jeschke M, Baumgartner S, Legewie S (2013). Determinants of cell-to-cell variability in protein kinase signaling. PLoS Comput Biol 9, e1003357.

Lauer P, Chow MY, Loessner MJ, Portnoy DA, Calendar R (2002). Construction, characterization, and use of two *Listeria monocytogenes* site-specific phage integration vectors. J Bacteriol 184, 4177–4186.

Loewer A, Lahav G (2011). We are all individuals: causes and consequences of non-genetic heterogeneity in mammalian cells. Curr Opin Genet Dev 21, 753–758.

Mengaud J, Ohayon H, Gounon P, Mege RM, Cossart P (1996). E-cadherin is the receptor for internalin, a surface protein required for entry of *L. monocytogenes* into epithelial cells. Cell 84, 923–932.

Pentecost M, Kumaran J, Ghosh P, Amieva MR (2010). Listeria monocytogenes internalin B activates junctional endocytosis to accelerate intestinal invasion. PLoS Pathog 6, e1000900.

Portnoy DA, Auerbuch V, Glomski IJ (2002). The cell biology of *Listeria monocytogenes* infection: the intersection of bacterial pathogenesis and cell-mediated immunity. J Cell Biol 158, 409–414.

Portnoy DA, Jacks PS, Hinrichs DJ (1988). Role of hemolysin for the intracellular growth of *Listeria monocytogenes*. J Exp Med 167, 1459–1471.

Purvis JE, Lahav G (2013). Encoding and decoding cellular information through signaling dynamics. Cell 152, 945–956.

Rengarajan M, Hayer A, Theriot JA (2016). Endothelial cells use a formin-dependent phagocytosis-like process to internalize the bacterium *Listeria monocytogenes*. PLoS Pathog 12, e1005603.

Robbins JR, Barth AI, Marquis H, De Hostos EL, Nelson WJ, Theriot JA (1999). *Listeria monocytogenes* exploits normal host cell processes to spread from cell to cell. J Cell Biol 146, 1333–1350.

Shen A, Higgins DE (2005). The 5′ untranslated region-mediated enhancement of intracellular listeriolysin O production is required for Listeria monocytogenes pathogenicity. Mol Microbiol 57, 1460–1473.

Sigal A, Milo R, Cohen A, Geva-Zatorsky N, Klein Y, Liron Y, Rosenfeld N, Danon T, Perzov N, Alon U (2006). Variability and memory of protein levels in human cells. Nature 444, 643–646.

Snijder B, Pelkmans L (2011). Origins of regulated cell-to-cell variability. Nat Rev Mol Cell Biol 12, 119–125.

Snijder B, Sacher R, Ramo P, Damm EM, Liberali P, Pelkmans L (2009). Population context determines cell-to-cell variability in endocytosis and virus infection. Nature 461, 520–523.

Spudich JL, Koshland DE JR (1976). Non-genetic individuality: chance in the single cell. Nature 262, 467–471.

Tilney LG, Portnoy DA (1989). Actin filaments and the growth, movement, and spread of the intracellular bacterial parasite, Listeria monocytogenes. J Cell Biol 109, 1597–1608.

Yam PT, Theriot JA (2004). Repeated cycles of rapid actin assembly and disassembly on epithelial cell phagosomes. Mol Biol Cell 15, 5647–5658.

Zeldovich VB, Robbins JR, Kapidzic M, Lauer P, Bakardjiev AI (2011). Invasive extravillous trophoblasts restrict intracellular growth and spread of Listeria monocytogenes. PLoS Pathog 7, e1002005.